

RSC Advances



This is an *Accepted Manuscript*, which has been through the Royal Society of Chemistry peer review process and has been accepted for publication.

Accepted Manuscripts are published online shortly after acceptance, before technical editing, formatting and proof reading. Using this free service, authors can make their results available to the community, in citable form, before we publish the edited article. This *Accepted Manuscript* will be replaced by the edited, formatted and paginated article as soon as this is available.

You can find more information about *Accepted Manuscripts* in the [Information for Authors](#).

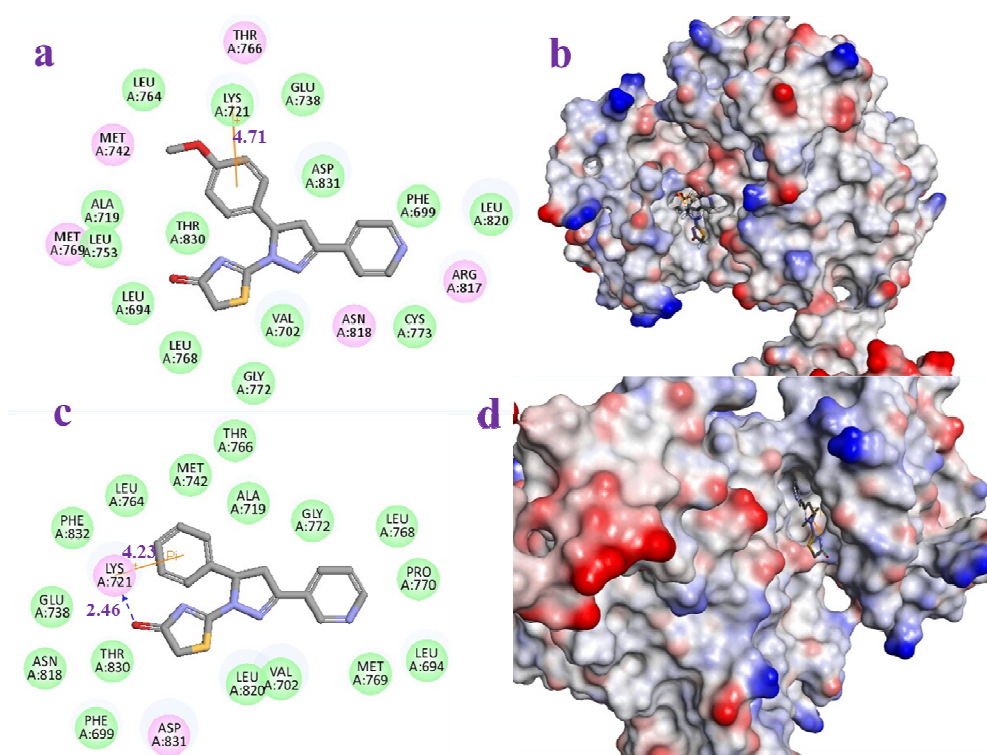
Please note that technical editing may introduce minor changes to the text and/or graphics, which may alter content. The journal's standard [Terms & Conditions](#) and the [Ethical guidelines](#) still apply. In no event shall the Royal Society of Chemistry be held responsible for any errors or omissions in this *Accepted Manuscript* or any consequences arising from the use of any information it contains.

EGFR/HER-2 Inhibitors: Synthesis, Biological Evaluation, 3D – QSAR Analysis of Dihydropyridin Containing Thiazolinone Derivatives

Yu-Jia Ren^{a†}, Zhong-Chang Wang^{a†}, Xin Zhang^a, Han-Yue Qiu^a, Peng-Fei Wang^a, Ai-Qin Jiang^{b*}, Hai-Liang Zhu^{a*}

^aState Key Laboratory of Pharmaceutical Biotechnology, Nanjing University, Nanjing 210093, People's Republic of China

^bMedical School of Nanjing University, Nanjing 210093, People's Republic of China



Docking of compound **4o** and **4g** in the ATP binding site of EGFR: Left: 2D model of the interaction between compound **4o**, **4g** and the ATP binding site. Right: 3D model of the interaction between compound **4o**, **4g** and the ATP binding site, respectively.

**EGFR/HER-2 Inhibitors: Synthesis, Biological Evaluation, 3D –
QSAR Analysis of Dihydropyridin Containing Thiazolinone
Derivatives**

**Yu-Jia Ren^{a†}, Zhong-Chang Wang^{a†}, Xin Zhang^a, Han-Yue Qiu^a,
Peng-Fei Wang^a, Ai-Qin Jiang^{b*}, Hai-Liang Zhu^{a*}**

*^aState Key Laboratory of Pharmaceutical Biotechnology, Nanjing University, Nanjing
210093, People's Republic of China*

^bMedical School of Nanjing University, Nanjing 210093, People's Republic of China

*Corresponding author. Tel. & fax: +86-25-83592672; e-mail: zhuhl@nju.edu.cn.

†These two authors equally contributed to this paper.

Abstract

A series of dihydropyridin containing thiazolinone derivatives (**4a-4r**) have been designed, synthesized and their biological activities were also evaluated as potential EGFR and HER-2 kinase inhibitors and tumor cell antiproliferation. All these synthesized compounds were determined by ¹H-NMR and MS. In addition, **4m** compounds were scrutinized by X-ray structure analysis. Among them, compound **4r** displayed the most potent inhibitory activity (IC₅₀ = 0.07 μM for EGFR and IC₅₀ = 0.26 μM for HER-2). Antiproliferative assay results indicated that compound **4r** owned high antiproliferative activity against B16-F10, Hela and MCF-7 *in vitro*, with IC₅₀ value of 0.09 μM, 0.29 μM, and 0.56 μM, respectively. Docking simulation was further performed to position compound **4r** into the EGFR active site to determine the probable binding model the 3D-QSAR models were built for reasonable design of EGFR/HER-2 inhibitors at present and in future.

Keywords:

Dihydropyridin
Thiazolinone
Synthesis
EGFR/HER-2
3D - QSAR

1. Introduction

As the research moves along, cancer chemotherapy ushers in a new period of vigorous development: molecular-targeted therapeutics have emerged which are highly selective and less toxic compared to the traditional drugs.^{1,2} STI571 exemplifies the successful development of these novel anticancer drugs which are those targeting aberrantly expressed oncogenic growth factor receptor involved in proliferative signal transduction pathways in cancer cells.^{3,4} Receptor protein tyrosine kinases (RPTKs) play a fundamental role in signal transduction pathways that mediate malignant cell transformation. Epidermal growth factor receptor kinase (EGFR), a transmembrane PTK that is activated by ligand-induced dimerization, plays a key role in the formation and development of many types of solid tumors, including head and neck, lung, breast, bladder, prostate, and kidney cancers. Therefore, EGFR tyrosine kinase represents an attractive target for the development of novel anticancer agents.^{5,6} (EGFR) and the homologous HER-2 kinases, which are members of the type 1 or erbB/HER receptor tyrosine kinase (RTK) family, have emerged as the most viable anticancer molecular targets in this family of four members, EGFR (HER-1/ErbB-1), HER-2 (ErbB-2/neu), HER-3 (ErbB-3), and HER-4 (ErbB-4).^{2,7,8} Among them, EGFR and HER-2 are the hottest targets in current cancer research and their overexpression or abnormal activation often cause cell malignant transformation, such as non small cell lung cancer (NSCLC), prostate, breast, stomach, colon, and ovarian cancers.⁹⁻¹⁰ Compounds that inhibit the kinase activity of EGFR and/or HER-2 after binding of its ATP binding site are of potential interest as new therapeutic antitumor agents.¹¹ Several EGFR inhibitors, the first-generation EGFR inhibitors **Gefitinib** (IressaTM)¹² and **Erlotinib** (TarcevaTM)¹³ have been approved by US FDA for treatment of patients with non small cell lung cancer (NSCLC). And **Lapatinib** as a dual reversible EGFR/HER2 inhibitor was approved for breast cancer therapy.¹² Two candidate drugs **Afatinib**¹⁴ and **Dacomitinib**,¹⁵ which could bond with a unique cysteine797 residue located at the lip of the ATP binding cleft[13], as the most promising second generation EGFR kinase inhibitors, have been being evaluated in respective phase III study.¹⁶ (**Fig. 1**)

In previous study, pyridine derivatives have been selected as pharmacological agents due to their biological activities and their potential applications.¹⁷ The application of this heterocycle is widespread due to its antiviral/antitumor,^{16,18-20} antibacterial,^{21,22} antiinflammatory,²³ fungistatic,²⁴ and anti-hyperglycemic activity.²⁵

Furthermore, special attention has been placed recently on the use of pyrazole for anticancer. Recently, a series of novel pyrazole derivatives containing thiourea skeleton (**PD, Fig. 1**) were discovered as potent anticancer agents targeting EGFR TK in our group, and some of them had demonstrated potent antitumor activity.^{26,27}

Thiazolinone and their derivatives have attracted continuing interest over the years because of their varied biological activities, such as anti-inflammatory, antimicrobial, antiproliferative, antiviral, anticonvulsant, antifungal, and antibacterial.²⁸⁻³² Recent years, thiazolinone derivatives with their antitumor activity have become a new hot spot. For example, thiazolinone containing benzothiazole moiety has been shown to exert its anticancer activity on leukemia, melanoma, lung, colon, CNS, ovarian, renal,

prostate and breast cancers cell lines by Dmytro Havrylyuk *et al.*³³ Besides these, many pyrazole or thiazolinone derivatives have also been reported potent biological activities and low toxicities.³⁴⁻³⁶ Encouraged by these observations we designed and synthesized newer anticancer compound derivatives which contains pyridine, pyrazole and thiazolinone.

Herein, each of the dihydropyridin containing thiazolinone and pyridine derivatives prepared has been tested for their biological activities as potential EGFR and HER-2 kinase inhibitors and the results are reported in this paper.

2. Results and discussion

2.1. Chemistry

All novel dihydropyridin containing thiazolinone (**4a-4r**) derivatives were synthesized following the synthetic pathway depicted in **Scheme 1**^a. The starting diverse substituted chalcones (**2a-2r**) were synthesized by Pyridinecarboxaldehyde and the substituted acetophenone in the presence of excess sodium hydroxide, using 40% sodium hydroxide as catalyst in water. Then the reaction of cyclization of different chalcones with thiosemicarbazide in refluxing ethanol, in the presence of excess sodium hydroxide, afforded the formation of dihydropyridin derivatives containing thiourea skeleton (**3a-3r**). Finally, the condensation of dihydropyridin derivatives containing thiourea skeleton with the appropriate ethyl bromoacetate and sodium acetate was used as acid-binding agent, keeping under stirring at 80 °C for 8h, resulted in the formation of dihydropyridin containing thiazolinone derivatives (**4a-4r**). All of the target compounds gave satisfactory analytical and spectroscopic data, which in accordance with their depicted structures by ¹H NMR, MS.

2.2. Crystal structures of compound **4m**

Among these compounds, the crystal structure of compound **4m** was determined by X-ray diffraction analysis. The crystallographic data for the structural analysis have been presented in **Table 1** and **Fig. 2**.

2.3. Biological activity

2.3.1. Antiproliferation assay

In the present work, eighteen of the newly synthesized derivatives **4a - 4r** were evaluated on their in vitro growth inhibitory activities against three cultured cell lines, which are B16-F10, Hela and MCF-7 in comparison to the known anticancer drugs: **Gefitinib** and **Celecoxib** as reference drugs. The outcomes were summarized up in **Table 2**. As shown in **Table 2**, the results revealed that most of the synthesized compounds exhibited significant anticancer activities, ranging from 0.09 to 8.29 μ M, with regard to broad-spectrum antitumor activity. Especially on MCF-7 cell proliferation activity. Among them, compound **4f** displayed the most potent anti-tumor activity in MCF-7 with IC_{50} of 0.15 μ M, compared to the positive control Gefitinib (IC_{50} =6.70 μ M) and Celecoxib (IC_{50} =7.01 μ M). More potent anti-tumor activity for MCF-7 together with virtual screening results both indicated that the EGFR might be a potential target which these dihydropyridin containing thiazolinone derivatives interacted with.

2.3.2 EGFR and HER-2 inhibitory activity

All compounds were tested for their EGFR inhibition to EGFR and HER-2 using a

solid-phase ELISA assay, with **Erlotinib** as the positive control drug. In this assay, the IC_{50} values of compounds possessing sufficiently potent anti-cancer activity were shown in **Table 2**. The results were compared with that provided by the known anticancer: **Erlotinib** under identical conditions, which showed that most of the synthesized compounds exhibited significant anticancer activities.

The following structure-activity relationship (SAR) can be observed from data of **Table 3**, EGFR and HER-2 activities of these compounds were tested against the standard clinically used inhibitors **Erlotinib**. For the majority of the compounds, we found that compounds containing thiazolinone and dihydropyridin rings showed excellent inhibiting EGFR activities displaying IC_{50} values between 0.099 and 19.62 μM . Compound **4o** was the most active having IC_{50} value of 0.099 μM , whereas compound **4d** was the least active with IC_{50} value of 19.62 μM .

Based on the data obtained, we surveyed a variety of substituents at different positions on the pyridine and A- rings of these compounds **4a-4r** (**Scheme 1^a**), they could be divided into two subunits: R_1 (pyridine ring) and A- rings to discuss how the substituents of these compounds affect the EGFR inhibitory activities. First, We chose different pyridine ring as the research object, and the result showed that most compounds with a nitrogen atoms on the 4-position of pyridine ring manifested more potent activities than compounds with a nitrogen atoms on the 2-position and 3-position of pyridine ring, (such as **4o** (IC_{50} =0.099 μM) > **4i** (IC_{50} =0.18 μM) > **4c** (IC_{50} =0.30 μM); **4q** (IC_{50} =7.28 μM) > **4k** (IC_{50} =9.63 μM) > **4e** (IC_{50} =12.18 μM). In addition, we studied the same pyridine ring and different substituents of A- rings, deduced that the substituent on the *para*-position of the A- rings is kind of potent electron-donating groups rather than electron-withdrawing groups, the compounds gained better activity say, for example **4c** (IC_{50} =0.30 μM) > **4b** (IC_{50} =2.63 μM) > **4a** (IC_{50} =5.26 μM) > **4f** (IC_{50} =8.32 μM) > **4e** (IC_{50} =12.18 μM) > **4d** (IC_{50} =19.2 μM); **4o** (IC_{50} =0.099 μM) > **4n** (IC_{50} =1.23 μM) > **4m** (IC_{50} =3.12 μM) > **4r** (IC_{50} =5.19 μM) > **4q** (IC_{50} =7.28 μM) > **4p** (IC_{50} =15.23 μM), and the inhibitory activities increased in the following order: $\text{OCH}_3 > \text{CH}_3 > \text{H} > \text{Br} > \text{Cl} > \text{F}$. For the given compounds, it was observed that the IC_{50} value for inhibition of EGFR kinase was higher than that observed of HER-2 kinase. However, they had the same trends. It was possibly attributed to the fact that higher concentration of the purified EGFR kinase was used than HER-2 kinase in the enzyme assays. It is evident that there is also a reason-able correlation between the EGFR and HER-2 inhibitory activities; thus, this is not surprising in view of the high sequence homology of the catalytic domains of these two kinases.

From the above mentioned analysis, it could be indicated that thiazolinone, pyridine ring and dihydropyridin rings in the dihydropyridin containing thiazolinone derivatives might play an important role in the EGFR and HER-2 inhibitory activity.

In comparison, we found that these compounds, with electron-donating groups group on the A-ring (such as OCH_3 , CH_3), exhibited more potent anticancer activities than those have electron-withdrawing substituents (such as F). From the above-mentioned analysis, it could be concluded that the compounds with methoxy substituted A- ring were found to be the most favorable for the anticancer activity.

2.3.3. Cytotoxicity test

All the target compounds were evaluated for their toxicity against human kidney epithelial cell 293T with the median cytotoxic concentration (CC₅₀) data of tested compounds by the MTT assay. As displayed in **Table 4**, these compounds were tested at multiple doses to study the viability of macrophage. As shown in **Table 4**, 18 compounds demonstrated almost no cytotoxic activities *in vitro* against human kidney epithelial cell 293T.

2.4. Molecular docking

To gain better understanding on the potency of the 18 compounds, we examined the interaction of these compounds with EGFR by molecular docking, which was performed by simulation of the 18 compounds into the ATP binding site in EGFR. The protein structure of the EGFR was downloaded from the PDB (1M17.pdb)³⁷ and was preprocessed using the Schrodinger Protein Preparation Guide, hydrogens were added to the structure, H-bonds within the protein were optimized, and the protein was minimized to an rmsd of 0.3 Å. A 9.9 Å sphere of water molecules was added around the ligand and a short (3ps) dynamics run was carried out, followed by several cycles of minimization using Quanta/CHARMm. The entire protein- ligand- water complex was allowed to move during calculations.³⁸ The predicted binding interaction energy was used as the criterion for ranking. The estimated interaction energy of other synthesized compounds was ranging from -41.89 to -31.20 kcal/mol. The selected compounds of **4o** and **4g** had an estimated binding free energy of -41.89 kcal/mol, -40.44 kcal/mol, respectively. The binding model of compounds **4o**, **4g** and EGFR was depicted in **Fig.3**. The amino acid residues which had interaction with EGFR were labeled. In the binding mode, compound **4o** was nicely bound to the ATP binding site of EGFR hydrophobic interaction and binding was stabilized by a π -cation interaction (**4o** A: Lys 721). Besides, compound **4g** was also nicely bound to the ATP binding site of EGFR hydrophobic interaction and binding was stabilized by one hydrogen bonds (angle Lys 721:HE1 4g:O = 94.45°, distance = 2.46 Å), and a π -cation interaction (4g A: Lys 721). This molecular docking result, along with the biological assay data, suggested that compounds **4o** and **4g** were a potential inhibitor of EGFR.

2.5 3D-QSAR model³⁹

In order to acquire a systematic SAR profile on dihydropyridin containing thiazolinone derivatives(**4a-4r**) as antitumor agents and to explore the more powerful and selective dual EGFR inhibitors, 3D-QSAR model was built to choose activity conformation of the designed molecular and reasonably evaluated the designed molecules by using the corresponding pIC₅₀ values which were converted from the obtained IC₅₀ (μ M) values of EGFR inhibition and performed by built-in QSAR software of DS 3.5 (Discovery Studio 3.5, Accelrys, Co. Ltd). The way of this transformation was derived from anonline calculator developed from an Indian medicinal chemistry lab ([http://www.sanjeevslab.org/tools-IC₅₀.html](http://www.sanjeevslab.org/tools-IC50.html)). The training and test set was divided by the random diverse molecules method of DS3.5, in which the test set accounts for 22.22% while the training set was set to 77.78%. The training set

composes 14 agents and 4 agents were consisted of the relative test set. The success of this model depended on docking study and the reliability of previous study about activities data.

In default situation, the alignment conformation of each molecule that possessed the lowest CDOCKER_INTERACTION_ENERGY among the eighteen docked poses. The 3D-QSAR model generated from DS 3.5, defined the critical regions (steric or electrostatic) affecting the binding affinity. It was a PLS model set up 400 independent variables (conventional $R^2 = 0.99$). The graphical relationship of observed and predicted values had been illustrated in **Fig. 4a**, in which the plot of the observed IC_{50} versus the predicted values showed that this model could be used in prediction of activity for dihydropyridin containing thiazolinone derivatives (**4a-4r**).

A contour plot of the electrostatic field region favorable (in blue) or unfavorable (red) for anticancer activity based on EGFR protein target were shown in **Fig. 4b** while the energy grids corresponding to the favorable (in green) or unfavorable (yellow) steric effects for the EGFR affinity were shown in **Fig. 4c**. It was widely acceptable that a better inhibitor based on the 3D-QSAR model should have strong Van der Waals attraction in the green areas and a polar group in the blue electrostatic potential areas (which were dominant close to the skeleton). As shown in these two pictures, this promising model would provide a guideline to design and optimize more effective EGFR inhibitors based on the dihydropyridin containing thiazolinone derivatives (**4a-4r**) and pave the way for us to further study in future.

3. Conclusions

In summary, we had designed and synthesized novel series of dihydropyridin containing thiazolinone derivatives (**4a-4r**) which had been tested for their anticancer activities against B16-F10, Hela and MCF-7 and EGFR/HER2 inhibitory activities. Most of them exhibited potent anticancer and EGFR/HER2 inhibitory activities, with IC_{50} ranging from 0.099-19.62 μM and 3.26-20.33 μM respectively. These compounds showed a very interesting profile for the inhibition of EGFR. Most of them exhibited EGFR inhibitory activities and almost no toxicity towards 293T. Among them, compound **4o** showed the most potent EGFR inhibition activities ($IC_{50} = 0.099 \mu\text{M}$ for EGFR and $IC_{50} = 3.26 \mu\text{M}$ for HER-2). Docking simulation was performed to get the probable binding models and poses. After analysis of the binding model of compounds **4o** and **4g** with EGFR, it was found that a hydrogen bond and a π -cation interaction with the protein residues in the ATP binding site might play a crucial role in its EGFR inhibition and antiproliferative activities. Finally, QSAR models were built with previous activity data and binding conformations to begin our work in this paper as well as to provide a reliable tool for reasonable design and synthesis of potent tyrosine kinase inhibitors.

4. Experiments

4.1 Materials and measurements

All chemicals and reagents used in current study were analytical grade. Thinlayer chromatography (TLC) was performed on silica gel plates with fluorescent indicator. All analytical samples were homogeneous on TLC in at least two different solvent systems. Melting points (uncorrected) were determined on a X-4 MP apparatus (Taike

Corp, Beijing, China). All the ^1H NMR spectra were recorded on a Bruker DPX 300 model Spectrometer in CDCl_3 and chemical shifts (δ) were reported as parts per million (ppm). ESI-MS spectra were recorded on a Mariner System 5304 Mass spectrometer.

4.2. Synthesis

4.2.1. General synthetic procedure of chalcones (**2a-2r**)

Equimolar portions of the appropriately Pyridinecarboxaldehyde (20 mmol) and substituted acetophenone (20 mmol) were dissolved in approximately 80 mL of ethanol. The mixture was allowed to stir for several minutes at 0 °C to dissolve. Subsequently added was 10 mmol aliquot of 40% aqueous sodium hydroxide solution dropwise to the reaction flask via a self-equalizing addition funnel. The reaction solution was allowed to stir at 0 °C for approximately 2 h, afterwards, the precipitate was collected by suction filtration. Washed by cold ethanol (30 mL) for three times, the purified chalcones (**2a-2r**) were acquired.

4.2.2. General synthetic procedure of pyrazole derivatives (**3a-3r**)

A mixture of chalcone (**2a-2r**, 10 mmol), thiosemicarbazide (10 mmol), and KOH (10 mmol) was added in a 150 mL flask, then refluxed in ethanol (75 mL) for 12 h. After cooling, the solution was poured into mass of ice-water and stirred for a few minutes. The precipitate formed was collected, washed three times with distilled water, and dried under vacuum. The crude products were purified by recrystallization with ethanol washed by ice-water (25 mL) for three times to give a pure product (**3a-3r**).

4.2.3. General synthetic procedure of dihydropyridin containing thiazolinone derivatives (**4a-4r**)

A mixture of compound **3a-3r** (5 mmol), bromoacetic acid (5 mmol), acetic anhydride (5 mmol), and sodium acetate (5 mmol) was dissolved in ethanol (30 mL) and kept stirring in 80 °C for 6-8 h. After cooling, the solution was poured into mass of ice-water and stirred for a few minutes. The precipitate formed was collected, washed three times with distilled water, and dried under vacuum. The crude products were purified by recrystallization with ethanol, methylene dichloride (1:1) washed by ice-water (25 mL) for three times to give a pure product (**4a-4r**)

4.2.3.1. 2-(5-Phenyl-3-(pyridin-2-yl)-4,5-dihydro-1H-pyrazol-1-yl)thiazol-4(5H)-one (**4a**)

Green solid, yield 63%, m.p. 189~191 °C; ^1H NMR (CDCl_3 , 300 MHz); δ : 8.55 (d, J = 3.2 Hz, 2H, Ar); 7.81 (d, J = 6.5 Hz, 2H, Ar); 7.70 (t, J = 6.9 Hz, 1H, Ar); 7.48 (d, J = 7.1 Hz, 4H, Ar); 5.91 (q, J = 9.1 Hz, 1H, CH); 3.95 (q, J = 8.3 Hz, 1H, CH); 3.87 (s, 2H, CH_2); 3.79 (q, J = 9.2 Hz, 1H, CH). ESI-MS: 323.3 ($\text{C}_{17}\text{H}_{14}\text{N}_4\text{OS}$ [$\text{M}+\text{H}$] $^+$).

4.2.3.2.

2-(3-(Pyridin-2-yl)-5-(*p*-tolyl)-4,5-dihydro-1H-pyrazol-1-yl)thiazol-4(5H)-one (**4b**)

Yellow solid. yield 53%, m.p. 147~149 °C; ^1H NMR (CDCl_3 , 300 MHz); δ : 8.56 (d, J = 5.3 Hz, 2H, Ar); 7.71 (d, J = 6.8 Hz, 2H, Ar); 7.47 (t, J = 2.0 Hz, 1H, Ar); 7.26 (d, J = 9.1 Hz, 3H, Ar); 5.91 (q, J = 6.2 Hz, 1H, CH); 3.87 (q, J = 8.2 Hz, 1H, CH); 3.74 (s, 2H, CH_2); 3.61 (q, J = 5.1 Hz, 1H, CH); 2.42 (s, 3H, CH_3). ESI-MS: 337.2 ($\text{C}_{18}\text{H}_{16}\text{N}_4\text{OS}$ [$\text{M}+\text{H}$] $^+$).

4.2.3.3.

2-(5-(4-Methoxyphenyl)-3-(pyridin-2-yl)-4,5-dihydro-1H-pyrazol-1-yl)thiazol-4(5H)-one (**4c**)

Yellow solid. yield 62%, m.p. 154~156°C; ¹H NMR (CDCl₃, 300 MHz); δ: 8.60 (d, *J* = 6.3 Hz, 2H, Ar); 7.78 (d, *J* = 9.9 Hz, 2H, Ar); 7.56 (t, *J* = 2.9 Hz, 1H, Ar); 6.92 (d, *J* = 5.1 Hz, 3H, Ar); 5.83 (q, *J* = 4.1 Hz, 1H, CH); 3.93 (q, *J* = 5.3 Hz, 1H, CH); 3.88 (d, *J* = 4.1 Hz, 3H, OCH₃); 3.86 (s, 2H, CH₂); 3.79 (q, *J* = 6.2 Hz, 1H, CH). ESI-MS: 353.1 (C₁₈H₁₆N₄O₂S [M+H]⁺).

4.2.3.4.

2-(5-(4-Fluorophenyl)-3-(pyridin-2-yl)-4,5-dihydro-1H-pyrazol-1-yl)thiazol-4(5H)-one (**4d**)

Yellow solid. Yield 67%, m.p. 162~164°C; ¹H NMR (CDCl₃, 300 MHz); δ: 8.67 (d, *J* = 4.5 Hz, 2H, Ar); 7.85 (d, *J* = 3.2 Hz, 2H, Ar); 7.69 (t, *J* = 7.9 Hz, 1H, Ar); 7.28 (d, *J* = 3.4 Hz, 3H, Ar); 5.89 (q, *J* = 4.7 Hz, 1H, CH); 3.93 (q, *J* = 4.8 Hz, 1H, CH); 3.88 (s, 2H, CH₂); 3.80 (q, *J* = 5.1 Hz, 1H, CH). ESI-MS: 341.21 (C₁₇H₁₃FN₄OS [M+H]⁺).

4.2.3.5.

2-(5-(4-Chlorophenyl)-3-(pyridin-2-yl)-4,5-dihydro-1H-pyrazol-1-yl)thiazol-4(5H)-one (**4e**)

Yellow solid. Yield 57%, m.p. 142~144°C; ¹H NMR (CDCl₃, 300 MHz); δ: 8.54 (d, *J* = 6.2 Hz, 2H, Ar); 7.78 (d, *J* = 7.3 Hz, 2H, Ar); 7.73 (t, *J* = 8.1 Hz, 1H, Ar); 7.36 (d, *J* = 6.4 Hz, 3H, Ar); 5.86 (q, *J* = 6.7 Hz, 1H, CH); 3.99 (q, *J* = 5.3 Hz, 1H, CH); 3.92 (s, 2H, CH₂); 3.84 (q, *J* = 8.2 Hz, 1H, CH). ESI-MS: 358.0 (C₁₇H₁₃ClN₄OS [M+H]⁺).

4.2.3.6.

2-(5-(4-Bromophenyl)-3-(pyridin-2-yl)-4,5-dihydro-1H-pyrazol-1-yl)thiazol-4(5H)-one (**4f**)

Yellow solid. Yield 51%, m.p. 183~186°C; ¹H NMR (CDCl₃, 300 MHz); δ: 8.48 (d, *J* = 3.3 Hz, 2H, Ar); 7.73 (d, *J* = 7.6 Hz, 2H, Ar); 7.68 (t, *J* = 4.3 Hz, 1H, Ar); 7.34 (d, *J* = 5.4 Hz, 3H, Ar); 5.88 (q, *J* = 5.1 Hz, 1H, CH); 3.89 (q, *J* = 9.8 Hz, 1H, CH); 3.68 (s, 2H, CH₂); 3.48 (q, *J* = 5.1 Hz, 1H, CH). ESI-MS: 401.1 (C₁₇H₁₃BrN₄OS [M+H]⁺).

4.2.3.7. 2-(5-Phenyl-3-(pyridin-3-yl)-4,5-dihydro-1H-pyrazol-1-yl)thiazol-4(5H)-one (**4g**)

Yellow solid. Yield 59%, m.p. 134~135°C; ¹H NMR (CDCl₃, 300 MHz); δ: 8.59 (d, *J* = 4.7 Hz, 2H, Ar); 7.92 (d, *J* = 5.4 Hz, 2H, Ar); 7.81 (t, *J* = 8.9 Hz, 1H, Ar); 7.51 (d, *J* = 5.1 Hz, 4H, Ar); 5.81 (q, *J* = 3.1 Hz, 1H, CH); 3.89 (q, *J* = 7.3 Hz, 1H, CH); 3.84 (s, 2H, CH₂); 3.76 (q, *J* = 7.2 Hz, 1H, CH). ESI-MS: 323.3 (C₁₇H₁₄N₄OS [M+H]⁺).

4.2.3.8. 2-(3-(Pyridin-3-yl)-5-p-tolyl-4,5-dihydro-1H-pyrazol-1-yl)thiazol-4(5H)-one (**4h**)

Yellow solid. Yield 71%, m.p. 147~149°C; ¹H NMR (CDCl₃, 300 MHz); δ: 8.57 (d, *J* = 2.6 Hz, 2H, Ar); 7.69 (d, *J* = 8.2 Hz, 2H, Ar); 7.59 (t, *J* = 2.0 Hz, 1H, Ar); 7.27 (d, *J* = 9.1 Hz, 3H, Ar); 5.82 (q, *J* = 4.1 Hz, 1H, CH); 3.99 (q, *J* = 11.3 Hz, 1H, CH); 3.89 (s, 2H, CH₂); 3.41 (q, *J* = 4.2 Hz, 1H, CH); 2.44 (s, 3H, CH₃). ESI-MS: 337.1 (C₁₈H₁₆N₄OS [M+H]⁺).

4.2.3.9.

2-(5-(4-Methoxyphenyl)-3-(pyridin-3-yl)-4,5-dihydro-1H-pyrazol-1-yl)thiazol-4(5H)-one (**4i**)

Yellow solid. Yield 54%, m.p. 143~144°C; $^1\text{H NMR}$ (CDCl_3 , 300 MHz); δ : 8.57 (d, $J = 3.3$ Hz, 2H, Ar); 7.81 (d, $J = 7.9$ Hz, 2H, Ar); 7.36 (t, $J = 4.9$ Hz, 1H, Ar); 6.72 (d, $J = 8.1$ Hz, 3H, Ar); 5.81 (q, $J = 3.1$ Hz, 1H, CH); 3.89 (q, $J = 8.3$ Hz, 1H, CH); 3.86 (d, $J = 3.1$ Hz, 3H, OCH_3); 3.82 (s, 2H, CH_2); 3.74 (q, $J = 8.2$ Hz, 1H, CH). ESI-MS: 353.3 ($\text{C}_{18}\text{H}_{16}\text{N}_4\text{O}_2\text{S}$ $[\text{M}+\text{H}]^+$).

4.2.3.10.

2-(5-(4-Fluorophenyl)-3-(pyridin-3-yl)-4,5-dihydro-1H-pyrazol-1-yl)thiazol-4(5H)-one (**4j**)

Yellow solid. Yield 52%, m.p. 154~155°C; $^1\text{H NMR}$ (CDCl_3 , 300 MHz); δ : 8.69 (d, $J = 6.1$ Hz, 2H, Ar); 7.91 (d, $J = 8.2$ Hz, 2H, Ar); 7.72 (t, $J = 6.3$ Hz, 1H, Ar); 7.39 (d, $J = 5.4$ Hz, 3H, Ar); 5.85 (q, $J = 6.2$ Hz, 1H, CH); 3.98 (q, $J = 5.7$ Hz, 1H, CH); 3.87 (s, 2H, CH_2); 3.81 (q, $J = 7.1$ Hz, 1H, CH). ESI-MS: 341.2 ($\text{C}_{17}\text{H}_{13}\text{FN}_4\text{OS}$ $[\text{M}+\text{H}]^+$).

4.2.3.11 2-(5-(4-Chlorophenyl)-3-(pyridin-3-yl)-4,5-dihydro-1H-pyrazol-1-yl)thiazol-4(5H)-one (**4k**)

Yellow solid. Yield 73%, m.p. 187~189°C; $^1\text{H NMR}$ (CDCl_3 , 300 MHz); δ : 8.57 (d, $J = 5.4$ Hz, 2H, Ar); 7.74 (d, $J = 8.5$ Hz, 2H, Ar); 7.58 (d, $J = 7.6$ Hz, 2H, Ar); 7.48 (d, $J = 8.4$ Hz, 3H, Ar); 5.86 (q, $J = 3.8$ Hz, 1H, CH); 4.02 (q, $J = 11.5$ Hz, 1H, CH); 3.89 (s, 2H, CH_2); 3.41 (q, $J = 4.0$ Hz, 1H, CH). ESI-MS: 357.9 ($\text{C}_{17}\text{H}_{13}\text{ClN}_4\text{OS}$ $[\text{M}+\text{H}]^+$).

4.2.3.12.

2-(5-(4-Bromophenyl)-3-(pyridin-3-yl)-4,5-dihydro-1H-pyrazol-1-yl)thiazol-4(5H)-one (**4l**)

Yellow solid. Yield 67%, m.p. 157~159°C; $^1\text{H NMR}$ (CDCl_3 , 300 MHz); δ : 8.56 (d, $J = 5.0$ Hz, 2H, Ar); 7.66 (d, $J = 7.2$ Hz, 2H, Ar); 7.57 (t, $J = 11.0$ Hz, 2H, Ar); 7.27 (d, $J = 4.9$ Hz, 2H, Ar); 5.86 (q, $J = 3.9$ Hz, 1H, CH); 3.99 (q, $J = 11.4$ Hz, 1H, CH); 3.88 (s, 2H, CH_2); 3.42 (q, $J = 4.2$ Hz, 1H, CH). ESI-MS: 401.4 ($\text{C}_{17}\text{H}_{13}\text{BrN}_4\text{OS}$ $[\text{M}+\text{H}]^+$).

4.2.3.13. 2-(5-Phenyl-3-(pyridin-4-yl)-4,5-dihydro-1H-pyrazol-1-yl)thiazol-4(5H)-one (**4m**)

White solid. Yield 63%, m.p. 189~191°C; $^1\text{H NMR}$ (CDCl_3 , 300 MHz); δ : 8.55 (d, $J = 3.2$ Hz, 2H, Ar); 7.81 (d, $J = 6.5$ Hz, 2H, Ar); 7.70 (t, $J = 6.9$ Hz, 1H, Ar); 7.48 (d, $J = 7.1$ Hz, 4H, Ar); 5.91 (q, $J = 9.1$ Hz, 1H, CH); 3.95 (q, $J = 8.3$ Hz, 1H, CH); 3.87 (s, 2H, CH_2); 3.79 (q, $J = 9.2$ Hz, 1H, CH). ESI-MS: 323.3 ($\text{C}_{17}\text{H}_{14}\text{N}_4\text{OS}$ $[\text{M}+\text{H}]^+$).

4.2.3.14.

2-(3-(Pyridin-4-yl)-5-(p-tolyl)-4,5-dihydro-1H-pyrazol-1-yl)thiazol-4(5H)-one (**4n**)

Yellow solid. Yield 66%, m.p. 176~178°C; $^1\text{H NMR}$ (CDCl_3 , 300 MHz); δ : 8.62 (d, $J = 8.3$ Hz, 2H, Ar); 7.73 (d, $J = 6.8$ Hz, 2H, Ar); 7.64 (t, $J = 8.1$ Hz, 1H, Ar); 7.47 (d, $J = 5.1$ Hz, 3H, Ar); 5.79 (q, $J = 4.6$ Hz, 1H, CH); 4.02 (q, $J = 7.3$ Hz, 1H, CH); 3.91 (s, 2H, CH_2); 3.50 (q, $J = 6.1$ Hz, 1H, CH); 2.49 (s, 3H, CH_3). ESI-MS: 337.2 ($\text{C}_{18}\text{H}_{16}\text{N}_4\text{OS}$ $[\text{M}+\text{H}]^+$).

4.2.3.15.

2-(5-(4-Methoxyphenyl)-3-(pyridin-4-yl)-4,5-dihydro-1H-pyrazol-1-yl)thiazol-4(5H)-one (**4o**)

Yellow solid. Yield 62%, m.p. 145~147°C; $^1\text{H NMR}$ (CDCl_3 , 300 MHz); δ : 8.59 (d, $J = 3.9$ Hz, 2H, Ar); 7.75 (d, $J = 8.6$ Hz, 2H, Ar); 7.29 (t, $J = 3.8$ Hz, 1H, Ar); 6.99 (d, $J = 4.1$ Hz, 3H, Ar); 5.79 (q, $J = 3.1$ Hz, 1H, CH); 3.99 (q, $J = 11.3$ Hz, 1H, CH); 3.87 (d,

$J = 5.1$ Hz, 3H, OCH₃); 3.85 (s, 2H, CH₂); 3.79 (q, $J = 4.2$ Hz, 1H, CH). ESI-MS: 353.2 (C₁₈H₁₆N₄O₂S [M+H]⁺).

4.2.3.16.

2-(5-(4-Fluorophenyl)-3-(pyridin-4-yl)-4,5-dihydro-1H-pyrazol-1-yl)thiazol-4(5H)-one (**4p**)

Yellow solid. Yield 47%, m.p. 172~174 °C; ¹H NMR (CDCl₃, 300 MHz); δ : 8.64 (d, $J = 5.4$ Hz, 2H, Ar); 7.87 (d, $J = 5.1$ Hz, 2H, Ar); 7.79 (t, $J = 6.2$ Hz, 1H, Ar); 7.34 (d, $J = 6.2$ Hz, 3H, Ar); 5.81 (q, $J = 7.8$ Hz, 1H, CH); 3.98 (q, $J = 5.2$ Hz, 1H, CH); 3.86 (s, 2H, CH₂); 3.77 (q, $J = 3.4$ Hz, 1H, CH). ESI-MS: 341.4 (C₁₇H₁₃FN₄OS [M+H]⁺).

4.2.3.17.

2-(5-(4-Chlorophenyl)-3-(pyridin-4-yl)-4,5-dihydro-1H-pyrazol-1-yl)thiazol-4(5H)-one (**4q**)

Yellow solid. Yield 56%, m.p. 165~166 °C; ¹H NMR (CDCl₃, 300 MHz); δ : 8.63 (d, $J = 6.1$ Hz, 2H, Ar); 7.81 (d, $J = 7.5$ Hz, 2H, Ar); 7.63 (d, $J = 6.7$ Hz, 2H, Ar); 7.51 (d, $J = 10.4$ Hz, 3H, Ar); 5.83 (q, $J = 4.1$ Hz, 1H, CH); 4.04 (q, $J = 9.3$ Hz, 1H, CH); 3.92 (s, 2H, CH₂); 3.35 (q, $J = 4.3$ Hz, 1H, CH). ESI-MS: 357.7 (C₁₇H₁₃ClN₄OS [M+H]⁺).

4.2.3.18.

2-(5-(4-Bromophenyl)-3-(pyridin-4-yl)-4,5-dihydro-1H-pyrazol-1-yl)thiazol-4(5H)-one (**4r**)

Red solid. yield 55%, m.p. 166~168 °C; ¹H NMR (CDCl₃, 300 MHz); δ : 8.51 (d, $J = 5.3$ Hz, 2H, Ar); 7.64 (d, $J = 6.9$ Hz, 2H, Ar); 7.53 (t, $J = 9.1$ Hz, 2H, Ar); 7.41 (d, $J = 8.4$ Hz, 2H, Ar); 5.81 (q, $J = 6.1$ Hz, 1H, CH); 3.94 (q, $J = 3.7$ Hz, 1H, CH); 3.89 (s, 2H, CH₂); 3.49 (q, $J = 7.6$ Hz, 1H, CH). ESI-MS: 401.4 (C₁₇H₁₃BrN₄OS [M+H]⁺).

4.3. Preparation, purification of HER-2 and EGFR and inhibitory assay

A 1.7 Kb cDNA encoded for human HER-2 cytoplasmic domain (HER-2-CD, amino acids 676–1245) and 1.6 kb cDNA encoded for the EGFR cytoplasmic domain (EGFR-CD, amino acids 645–1186) were cloned into baculoviral expression vectors pBlueBacHis2B and pFASTBacHTc (Huakang Company, China), separately. A sequence that encodes (His)₆ was located at the 5' upstream to the HER-2 and EGFR sequences. Sf-9 cells were infected for 3 days for protein expression. Sf-9 cell pellets were solubilized at 0 °C in a buffer at pH 7.4 containing 50 mM HEPES, 10 mM NaCl, 1% Triton, 10 μ M ammonium molybdate, 100 μ M sodium vanadate, 10 μ g/mL aprotinin, 10 μ g/mL leupeptin, 10 μ g/mL pepstatin, and 16 μ g/mL benzamidine HCl for 20 min followed by 20 min centrifugation. Crude extract supernatant was passed through an equilibrated Ni-NTA superflow packed column and washed with 10 mM and then 100 mM imidazole to remove nonspecifically bound material. Histidine tagged proteins were eluted with 250 and 500 mM imidazole and dialyzed against 50 mM NaCl, 20 mM HEPES, 10% glycerol, and 1 μ g/mL each of aprotinin, leupeptin, and pepstatin for 2 h. The entire purification procedure was performed at 4 °C or on ice (Tsou, Mamuya et al. 2001).

Both EGFR and HER-2 kinase assays were set up to assess the level of autophosphorylation based on DELFIA/Time-Resolved Fluorometry. Compounds **4a-4r** were dissolved in 100% DMSO and diluted to the appropriate concentrations with 25 mM HEPES at pH 7.4. In each well, 10 μ L compound was incubated with

10 μ L (12.5 ng for HER-2 or 5 ng for EGFR) recombinant enzyme (1:80 dilution in 100 mM HEPES) for 10 min at room temperature. Then, 10 μ L of 5 mM buffer (containing 20 mM HEPES, 2 mM MnCl₂, 100 μ M Na₃VO₄, and 1 mM DTT) and 20 μ L of 0.1 mM ATP–50 mM MgCl₂ were added for 1 h. Positive and negative controls were included in each plate by incubation of enzyme with or without ATP–MgCl₂. At the end of incubation, liquid was aspirated, and plates were washed three times with wash buffer. A 75 μ L (400 ng) sample of europium labeled anti-phosphotyrosine antibody was added to each well for another 1 h of incubation. After washing, enhancement solution was added and the signal was detected by Victor (Wallac Inc.) with excitation at 340 nm and emission at 615 nm. The percentage of auto-phosphorylation inhibition by the compounds was calculated using the following formula: 100% - [(negative control)/ (positive control - negative control)]. The IC₅₀ was obtained from curves of percentage inhibition with eight concentrations of compound. As the contaminants in the enzyme preparation are fairly low, the majority of the signal detected by the anti-phosphotyrosine antibody is from EGFR or HER-2.

4.4. Antiproliferative activity

The antiproliferative activities of the prepared compounds were evaluated using a standard (MTT)-based colorimetric assay with some modification. Cell lines were grown to log phase in DMEM supplemented with 10% fetal bovine serum, under a humidified atmosphere of 5% CO₂ at 37 °C. Cell suspensions were prepared and 100 μ L/well dispensed into 96-well plates giving 10⁵ cells/well. The plates were returned to the incubator for 24 h to allow the cells to reattach. Subsequently, cells were treated with the target compounds at increasing concentrations in the presence of 10% FBS for 48 h. Then, cell viability was assessed by the conventional 3-(4,5-dimethylthiazol-2-yl)-2,5-diphenyltetrazolium bromide (MTT) reduction assay and carried out strictly according to the manufacturer instructions (Sigma). The absorbance (OD₅₇₀) was read on an ELISA reader (Tecan, Austria).

4.5. Molecular docking study

Docking of compounds into the 3D EGFR complex structure (PDB code: 1M17) was carried out using the Discovery Studio (version 3.5) as implemented through the graphical user interface DS-LigandFit protocol. The three-dimensional structures of the aforementioned compounds were constructed using Chem 3D ultra 11.0 software [Chemical Structure Drawing Standard; Cambridge Soft corporation, USA (2009)], then they were energetically minimized by using MOPAC with 100 iterations and minimum RMS gradient of 0.10. The crystal structures of EGFR complex were retrieved from the RCSB Protein Data Bank (<http://www.rcsb.org/pdb/home/home.do>). All bound water and ligands were eliminated from the protein and the polar hydrogen was added. The whole EGFR complex was defined as a receptor and the site sphere was selected based on the ligand binding location of ATP, then the ATP molecule was removed and **4o** and **4g** was placed during the molecular docking procedure. Types of interactions of the docked protein with ligand were analyzed after the end of molecular docking.

4.6. 3D-QSAR

Ligand-based 3D-QSAR approach was performed by QSAR software of DS 3.5

(Discovery Studio 3.5, Accelrys, Co.Ltd). The training sets were composed of inhibitors with the corresponding pIC₅₀ values which were converted from the obtained IC₅₀ (μ M), and test sets comprised compounds of data sets as list in **Table 4**.

In Discovery Studio, the CHARMM force field is used and the electrostatic potential and the van der Waals potential are treated as separate terms. A +1e point charge is used as the electrostatic potential probe and distance-dependent dielectric constant is used to mimic the solvation effect. For the van der Waals potential a carbon atom with a 1.73 Å radius is used as a probe.

All the definition of the descriptors can be seen in the “Help” of DS 3.5 software and they were calculated by QSAR protocol of DS 3.5. The alignment conformation of each molecule was the one with lowest interaction energy in the docked results of CDOCKER. The predictive ability of 3D-QSAR modeling can be evaluated based on the cross-validated correlation coefficient, which qualifies the predictive ability of the models. Scrambled test (Y scrambling) was performed to investigate the risk of chance correlations. The inhibitory potencies of compounds were randomly reordered for 30 times and subject to leave-one-out validation test, respectively. The models were also validated by test sets, in which the compounds are not included in the training sets, respectively. The models were also validated by test sets, in which the compounds are not included in the training sets. Usually, one can believe that the modeling is reliable, when the R² for test sets is larger than 0.6.

Acknowledgement

The work was financed by a grant (No. J1103512) from National Natural Science Foundation of China.

References and notes

- (1) Seymour, L. *Cancer. Treat. Rev.* **1999**, *25*, 301-312.
- (2) Kamath, S.; Buolamwini, J. K. *J. Med. Chem.* **2003**, *46*, 4657-4668.
- (3) Adjei, A. A. *J. Natl. Cancer. I.* **2001**, *93*, 1062-1074.
- (4) Druker, B. J. *Trends. Mol. Med.* **2002**, *8*, S14-S18.
- (5) Zhang, X.; Gureasko, J.; Shen, K.; Cole, P. A.; Kuriyan, J. *Cell.* **2006**, *125*, 1137-1149.
- (6) Xu, S.; Xu, T.; Zhang, L.; Zhang, Z.; Luo, J.; Liu, Y.; Lu, X.; Tu, Z.; Ren, X.; Ding, K. *J. Med. Chem.* **2013**, *56*, 8803-8813.
- (7) Rani, P.; Srivastava, V. K.; Kumar, A. *Eur. J. Med. Chem.* **2004**, *39*, 449-452.
- (8) Kolibaba, K. S.; Druker, B. J. *BBA-Rev. Cancer.* **1997**, *1333*, F217-F248.
- (9) Luo, Y.; Li, Y.; Qiu, K.; Lu, X.; Fu, J.; Zhu, H. *Bio. Med. Chem.* **2011**, *19*, 6069-6076.
- (10) Sridhar, S. S.; Seymour, L.; Shepherd, F. A. *Lancet Oncol.* **2003**, *4*, 397-406.
- (11) Bridges, A. J. *Cur. Med. Chem.* **1999**, *6*, 825-844.
- (12) Blume-Jensen, P.; Hunter, T. *Nature* **2001**, *411*, 355-365.
- (13) Ciardiello, F.; Tortora, G. *Clin. Cancer. Res.* **2001**, *7*, 2958-2970.
- (14) Boschelli, D. H. *Drug. Future.* **1999**, *24*, 515-538.
- (15) Chandregowda, V.; Venkateswara Rao, G.; Chandrasekara Reddy, G. *Org. Process. Res. Dev.* **2007**, *11*, 813-816.

- (16) Manfredini, S.; Bazzanini, R.; Baraldi, P. G.; Guarneri, M.; Simoni, D.; Marongiu, M. E.; Pani, A.; La Colla, P.; Tramontano, E. *J. Med. Chem.* **1992**, *35*, 917-924.
- (17) Abdel-Wahab, B. F.; Abdel-Aziz, H. A.; Ahmed, E. M. *Eur. J. Med. Chem.* **2009**, *44*, 2632-2635.
- (18) Solanki, J. S.; Thapak, T. R.; Bhardwaj, A.; Tripathi, U. N. *J. Coord. Chem.* **2011**, *64*, 369-376.
- (19) Manfredini, S.; Bazzanini, R.; Baraldi, P. G.; Bonora, M.; Marangoni, M.; Simoni, D.; Pani, A.; Scintu, F.; Pinna, E.; Pisano, L. *Anti-cancer. Drug. Des.* **1996**, *11*, 193-204.
- (20) Park, H.; Lee, K.; Park, S.; Ahn, B.; Lee, J.; Cho, H.; Lee, K. *Bioorg. Med. Chem. Lett.* **2005**, *15*, 3307-3312.
- (21) Tanitame, A.; Oyamada, Y.; Ofuji, K.; Fujimoto, M.; Iwai, N.; Hiyama, Y.; Suzuki, K.; Ito, H.; Terauchi, H.; Kawasaki, M. *J. Med. Chem.* **2004**, *47*, 3693-3696.
- (22) Güniz Küçükgül, Ş.; Rollas, S.; Erdeniz, H.; Kiraz, M.; Cevdet Ekin, A.; Vidin, A. *Eur. J. Med. Chem.* **2000**, *35*, 761-771.
- (23) Penning, T. D.; Talley, J. J.; Bertenshaw, S. R.; Carter, J. S.; Collins, P. W.; Docter, S.; Graneto, M. J.; Lee, L. F.; Malecha, J. W.; Miyashiro, J. M. *J. Med. Chem.* **1997**, *40*, 1347-1365.
- (24) Sridhar, R.; Perumal, P. T.; Etti, S.; Shanmugam, G.; Ponnuswamy, M. N.; Prabavathy, V. R.; Mathivanan, N. *Bioorg. Med. Chem. Lett.* **2004**, *14*, 6035-6040.
- (25) Bebernitz, G. R.; Argentieri, G.; Battle, B.; Brennan, C.; Balkan, B.; Burkey, B. F.; Eckhardt, M.; Gao, J.; Kapa, P.; Strohschein, R. J. *J. Med. Chem.* **2001**, *44*, 2601-2611.
- (26) Lv, P.; Li, H.; Sun, J.; Zhou, Y.; Zhu, H. *Bioorganic & medicinal chemistry* **2010**, *18*, 4606-4614.
- (27) Qiu, K.; Wang, H.; Wang, L.; Luo, Y.; Yang, X.; Wang, X.; Zhu, H. *Bioorg. Med. Chem.* **2012**, *20*, 2010-2018.
- (28) Webster, L. T.; Gilman, A.; Rall, T. W.; Nies, A. S.; Taylor, P. *In The Pharmacological Basis of the reapeutics; Pergamon Press: New York.* **1990**, *8th*, 999-1007.
- (29) Kundariya, D. S.; Patel, P. K.; Bheshdadia, B. M. *Chem. Sin.* **2014**, *5*, 138-143.
- (30) Geronikaki, A. A.; Pitta, E. P.; Liaras, K. S. *Cur. Med. Chem.* **2013**, *20*, 4460-4480.
- (31) Li, Y.; Geng, J.; Liu, Y.; Yu, S.; Zhao, G. *ChemMedChem* **2013**, *8*, 27-41.
- (32) Rydzik, E.; Szadowska, A.; Kamińska, A. *Acta. Pol. Pharm.* **1984**, *41*, 459-464.
- (33) Havrylyuk, D.; Zimenkovsky, B.; Karpenko, O.; Grellier, P.; Lesyk, R. Synthesis of pyrazoline-thiazolidinone hybrids with trypanocidal activity. *Eur. J. Med. Chem.* **2014**, *85*, 245-254.
- (34) Dayam, R.; Aiello, F.; Deng, J.; Wu, Y.; Garofalo, A.; Chen, X.; Neamati, N. *J. Med. Chem.* **2006**, *49*, 4526-4534.
- (35) Manfredini, S.; Bazzanini, R.; Baraldi, P. G.; Guarneri, M.; Simoni, D.; Marongiu, M. E.; Pani, A.; La Colla, P.; Tramontano, E. *J. Med. Chem.* **1992**, *35*, 917-924.
- (36) Manfredini, S.; Bazzanini, R.; Baraldi, P. G.; Bonora, M.; Marangoni, M.; Simoni, D.; Pani, A.; Scintu, F.; Pinna, E.; Pisano, L. *Anti-cancer. Drug. Des.* **1996**, *11*, 193-204.
- (37) Stamos, J.; Sliwkowski, M. X.; Eigenbrot, C. *J. Bio. Chem.* **2002**, *277*, 46265-46272.
- (38) Webster, L. T.; Gilman, A., Ed. Pergamon Press: New York., 1990; Vol. 8th, p 999-1007.
- (39) Egan, W. J.; Merz, K. M.; Baldwin, J. J. *J. Med. Chem.* **2000**, *43*, 3867-3877.

Figure Captions

Table 1. Crystal data for compound **4m**.

Table 2. In vitro anticancer activities (IC_{50} , μM) of compound **4a-4r** against human tumor cell lines.

Table 3. Inhibition activities of compounds **4a-4r** inhibit EGFR and HER-2.

Table 4. The median cytotoxic concentration (CC_{50}) data of all compounds.

Fig. 1 Selected EGFR/ HER-2 inhibitors.

Fig. 2. Crystal structure diagrams of compound **4m**.

Fig. 3 Docking of compound **4o** and **4g** in the ATP binding site of EGFR: Left: 2D model of the interaction between compound **4o**, **4g** and the ATP binding site. Right: 3D model of the interaction between compound **4o**, **4g** and the ATP binding site, respectively.

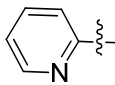
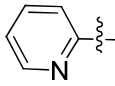
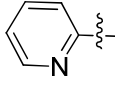
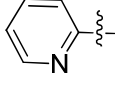
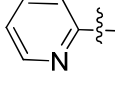
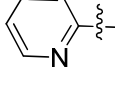
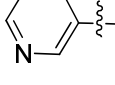
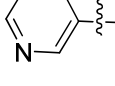
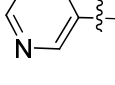
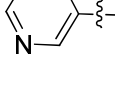
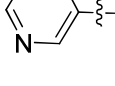
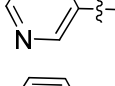
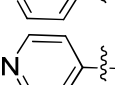
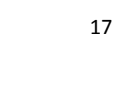
Fig. 4. (a) Using linear fitting curve to compare the predicted pIC_{50} value with that of experiment. (b) Isosurface of the 3D-QSAR model coefficients on electrostatic potential grids. The blue triangle mesh represents positive electrostatic potential and the red area represents negative electrostatic potential. (c) Isosurface of the 3D-QSAR model coefficients on Van der Waals grids. The green triangle mesh representation indicates positive coefficients; the yellow triangle mesh indicates negative coefficients.

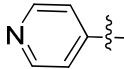
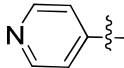
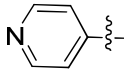
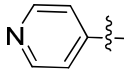
Scheme 1^a

Table 2. Crystal data for compound **4m**

Compound	4m
Empirical formula	C ₁₇ H ₁₄ N ₄ OS
Formula weight	322.8
Temperature(K)	273(2)
Crystal system	Monoclinic
Space group	<i>P</i> -1
<i>a</i> (Å)	7.7819(12)
<i>b</i> (Å)	10.0431(17)
<i>c</i> (Å)	10.0631(15)
α (°)	99.637(5)
β (°)	96.381(5)
γ (°)	99.610(5)
<i>V</i> (Å ³)	756.6(2)
<i>Z</i>	10
D _{calcd} /g cm ⁻³	1.4151(4)
θ rang (deg)	2.10 -27.50
F(000)	336.0
Reflections collected	8193 (<i>R</i> _{int} = 0.0304)
Data/restraints/parameters	3371 /0/ 208
Absorption coefficient (mm ⁻¹)	0.710
<i>R</i> ₁ ; <i>wR</i> ₂ [<i>I</i> > 2 σ (<i>I</i>)]	0.0444/ 0.1041
<i>R</i> ₁ ; <i>wR</i> ₂ (all data)	0.0686 / 0.1142
GOF	1.042
Larg.peak/hole(e. Å)	0.28/ -0.24

Table 2. In vitro anticancer activities (IC_{50} , μM) of compound **4a-4r** against human tumor cell lines.

Compounds	R_1	R_2	IC_{50} (μM) ^a		
			B16-F10 ^b	Hela ^b	MCF-7 ^b
4a	H		0.32	1.11	1.04
4b	CH ₃		1.88	2.39	1.96
4c	OCH ₃		4.12	5.17	3.55
4d	F		3.75	5.21	3.71
4e	Cl		3.24	5.68	2.55
4f	Br		0.19	0.21	0.15
4g	H		0.26	0.61	0.87
4h	CH ₃		1.22	1.95	0.83
4i	OCH ₃		3.41	5.19	2.64
4j	F		2.64	5.12	2.09
4k	Cl		2.14	3.13	2.65
4l	Br		0.41	0.11	0.23
4m	H		0.72	0.92	1.40
4n	CH ₃		2.02	3.08	1.57

4o	OCH ₃		5.52	8.29	3.76
4p	F		3.52	5.21	2.47
4q	Cl		3.37	5.03	2.73
4r	Br		0.09	0.29	0.56
Gefitinib	-	-	0.10	1.59	6.70
Celecoxib	-	-	5.28	7.51	7.01

^a Biological activity was measured using the MTT assay. Values are the average of three independent experiments run in triplicate. Variation was generally 5-10%.

^b Cancer cells kindly supplied by State Key Laboratory of Pharmaceutical Biotechnology, Nanjing University.

Table 3. Inhibition activities of compounds **4a-4r** inhibit EGFR and HER-2

Compounds	IC ₅₀ (μM) ^a		Compounds	IC ₅₀ (μM) ^a	
	EGFR ^b	HER-2 ^b		EGFR ^b	HER-2 ^b
4a	5.26	6.81	4k	9.63	12.38
4b	2.63	7.62	4l	5.42	5.03
4c	0.30	18.62	4m	3.12	4.95
4d	19.62	20.33	4n	1.23	4.83
4e	12.18	15.32	4o	0.099	3.26
4f	8.32	15.32	4p	15.23	18.32
4g	4.63	5.43	4q	7.28	8.63
4h	1.82	3.98	4r	5.19	5.08
4i	0.18	4.88	Erlotinib	0.03	0.14
4j	13.26	14.12			

^a Errors were in the range of (5-10% of the reported values, from three different assays).

^b Human recombinant enzymes, by the esterase assay (4-nitrophenylacetate as substrate).

Table 4. The median cytotoxic concentration (CC_{50}) data of all compounds.

Compounds	$CC_{50}^a, \mu\text{M}$	Compounds	$CC_{50}^a, \mu\text{M}$
4a	46.25	4k	43.28
4b	52.76	4l	53.44
4c	49.24	4m	49.21
4d	50.03	4n	52.36
4e	46.36	4o	63.23
4f	53.28	4p	43.28
4g	52.78	4q	55.64
4h	46.24	4r	57.38
4i	61.42	Celecoxib	53.46
4j	57.62		

^a The cytotoxicity of each compound was expressed as the concentration of compound that reduced cell viability to 50% (CC_{50}).

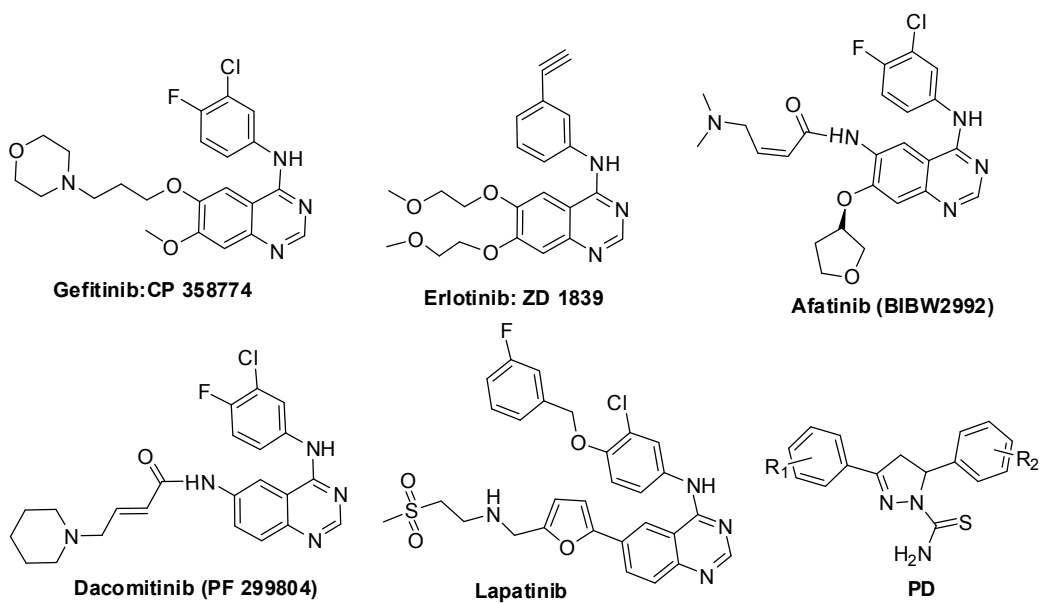


Fig. 1 Selected EGFR/ HER-2 inhibitors

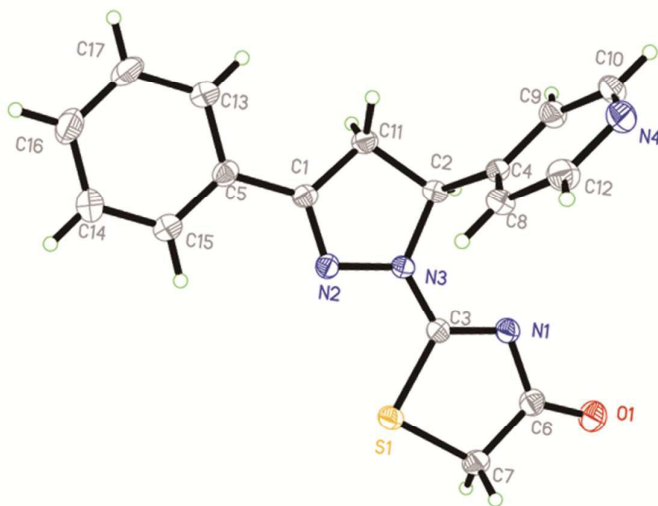


Fig. 2. Crystal structure diagrams of compound **4m**

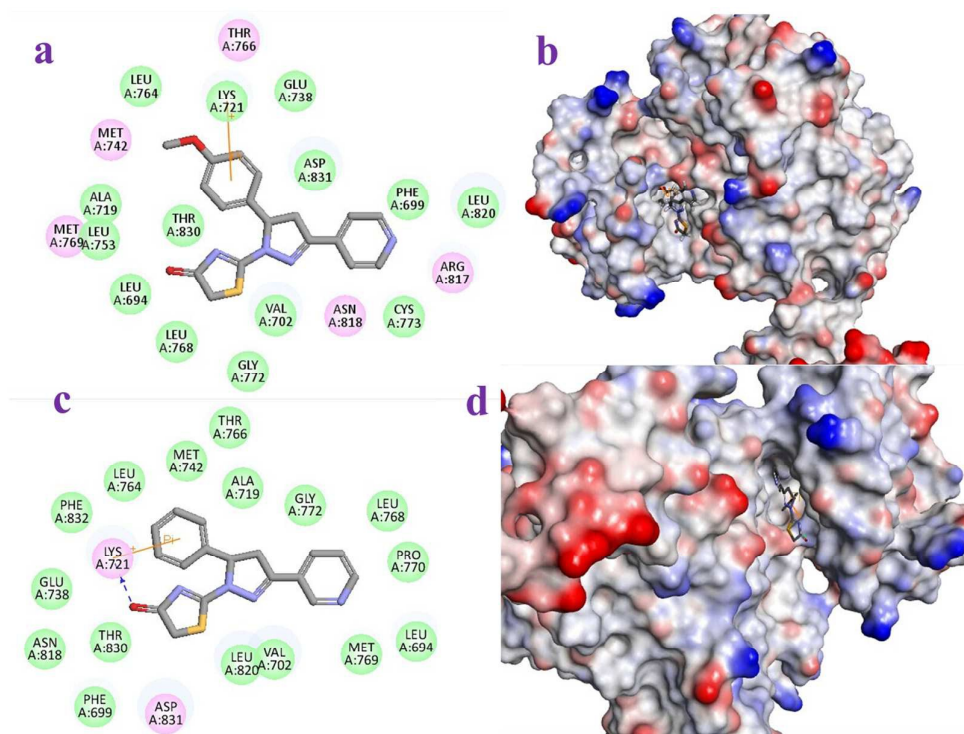


Fig. 3 Docking of compound **4o** and **4g** in the ATP binding site of EGFR: Left: 2D model of the interaction between compound **4o**, **4g** and the ATP binding site. Right: 3D model of the interaction between compound **4o**, **4g** and the ATP binding site, respectively.

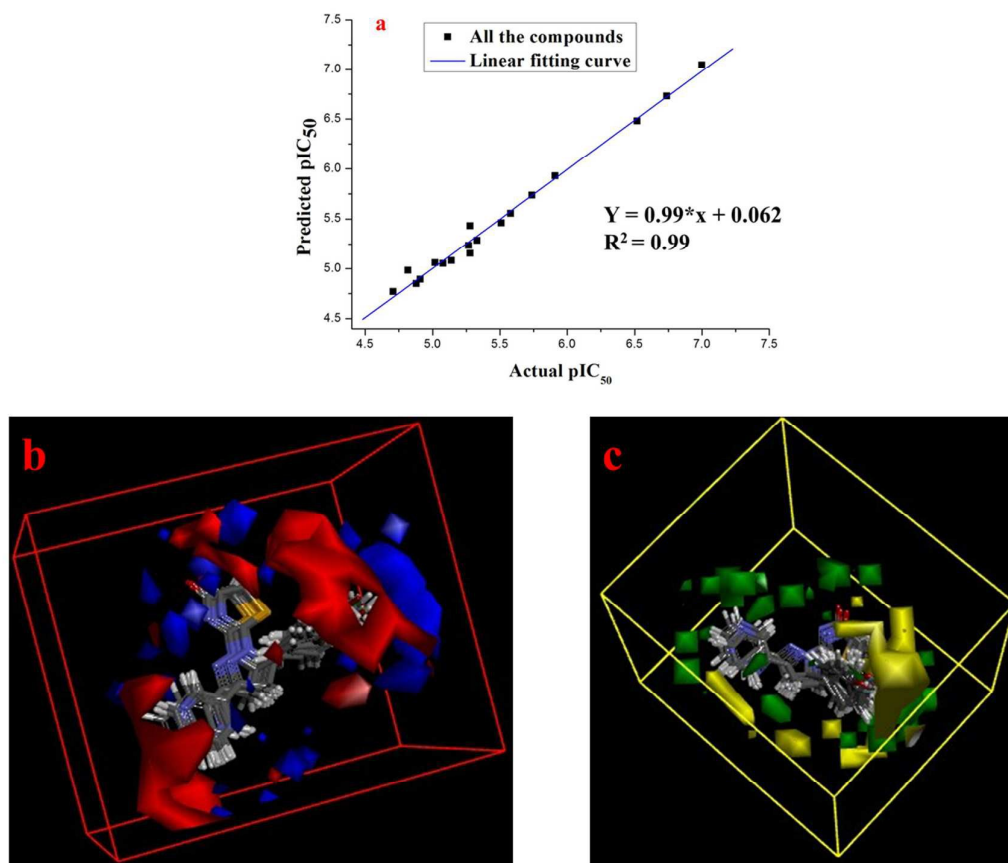
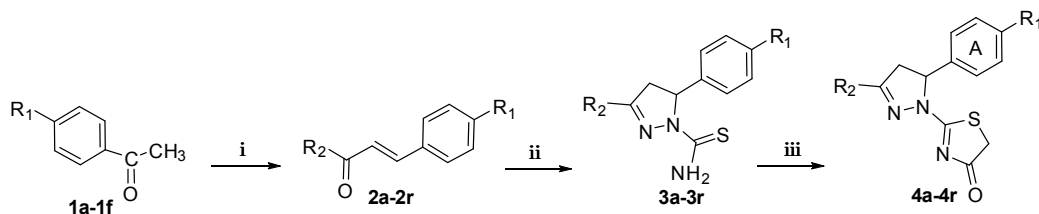


Fig. 4. (a) Using linear fitting curve to compare the predicted pIC_{50} value with that of experiment. (b) Isosurface of the 3D-QSAR model coefficients on electrostatic potential grids. The blue triangle mesh represents positive electrostatic potential and the red area represents negative electrostatic potential. (c) Isosurface of the 3D-QSAR model coefficients on Van der Waals grids. The green triangle mesh representation indicates positive coefficients; the yellow triangle mesh indicates negative coefficients

Scheme 1^a



^a Reagents and conditions: (i) 1.0 equiv Pyridinecarboxaldehyde, 40% aqueous potassium hydroxide solution, ethanol, 0 °C, 2 h, 62.6-78.2%; (ii) 1.0 equiv Thiosemicarbazide, KOH, ethanol, reflux; 12 h, 65.2-72.3%; (iii) Bromoacetic acid, acetic anhydride, sodium acetate, acetic acid, 80 °C, 8 h, 47.2-72.8%.